

# Clustering of MgII absorption line systems around massive galaxies: an important constraint on feedback processes in galaxy formation

Guinevere Kauffmann<sup>1\*</sup>, Dylan Nelson<sup>1</sup>, Brice Ménard<sup>2</sup>, Guangtun Zhu<sup>2</sup>

<sup>1</sup>*Max-Planck Institut für Astrophysik, 85741 Garching, Germany*

<sup>2</sup>*Department of Physics & Astronomy, Johns Hopkins University, Baltimore, MD, 21218, USA*

16 March 2017

## ABSTRACT

We use the latest version of the metal line absorption catalogue of Zhu & Ménard (2013) to study the clustering of MgII absorbers around massive galaxies ( $\sim 10^{11.5} M_{\odot}$ ), quasars and radio-loud AGN with redshifts between 0.4 and 0.75. Clustering is evaluated in two dimensions, by binning absorbers both in projected radius and in velocity separation. Excess MgII is detected around massive galaxies out to  $R_p = 20$  Mpc. At projected radii less than 800 kpc, the excess extends out to velocity separations of 10,000 km s<sup>-1</sup>. The extent of the high velocity tail within this radius is independent of the mean stellar age of the galaxy and whether or not it harbours an active galactic nucleus. We interpret our results using the publicly available Illustris and Millennium simulations. Models where the MgII absorbers trace the dark matter particle or subhalo distributions do not fit the data. They overpredict the clustering on small scales and do not reproduce the excess high velocity separation MgII absorbers seen within the virial radius of the halo. The Illustris simulations which include thermal, but not mechanical feedback from AGN, also do not provide an adequate fit to the properties of the cool halo gas within the virial radius. We propose that the large velocity separation MgII absorbers trace gas that has been pushed out of the dark matter halos, possibly by multiple episodes of AGN-driven mechanical feedback acting over long timescales.

**Key words:** galaxies:haloes; galaxies: formation; galaxies: structure ; galaxies: intergalactic medium

## 1 INTRODUCTION

An improved understanding of the distribution of gas in dark matter halos is key to solving the so-called “overcooling” problem in galaxy formation, which is based on the deduction that if gas simply cools over a Hubble time in dark matter halos in a universe dominated by cold dark matter, too many very high mass galaxies will be produced (White & Frenk 1991; Kauffmann, White & Guiderdoni 1993).

An important diagnostic of the ability of gas to cool comes from X-ray observations of groups and clusters. The deepest observations with the Chandra satellite now allow measurements of the gas mass fractions of groups as far out as  $r_{500}$  and it is found that the lowest mass systems have the lowest hot gas fractions (e.g. Sun et al 2009). One question has been to what extent these results are affected by the fact that the groups and clusters with deep X-ray observations

are almost always X-ray selected. In recent work, Anderson et al (2015) stacked a sample of 250,000 locally brightest galaxies from the Sloan Digital Sky Survey using data from the ROSAT All-Sky Survey, which was used to derive a relation between galaxy mass and average X-ray luminosity. Wang et al (2016) then used weak gravitational lensing to measure the total mass profiles around the same sample of stacked galaxies, thus allowing a derivation of the relation between X-ray luminosity and galaxy halo mass. The results yield a scaling between  $L_x$  and  $M_{500}$  that has a similar slope compared to previous work, but with a normalization that is a factor of 2 below the relations derived from X-ray selected samples.

These results suggest that there is considerable variation in the baryon content of halos at fixed galaxy mass. They also suggest that gas heating mechanisms play an important role in determining the *global* thermodynamic state of the gas in lower mass halos. McCarthy et al (2010) analyzed the predicted X-ray properties of X-ray groups in

\* E-mail: gamk@mpa-garching.mpg.de

cosmological hydrodynamical simulations from the Overwhelmingly Large Simulations (OWLS) project and showed that the models with AGN feedback produced X-ray scaling relations in much better agreement with observations than the models where the only gas heating mechanism is from supernovae. So far, however, X-ray observations are unable to constrain the physical nature of the heating process. Choi et al (2014,2015) compare two different AGN feedback models: one that includes only thermal heating, and another that includes mechanical feedback. The mechanical model was motivated by observations of winds in broad absorption line quasars (BAL QSOs), which convey energy, mass and momentum into the surrounding gas with velocity  $\sim 10,000$  km s $^{-1}$  (see Crenshaw, Kraemer & George 2003 for a review). Choi et al (2015) show that for a fixed amount of energy released during a given black hole accretion event, the mechanical model is much more efficient than the thermal model at pushing gas out of the central region of the halo and reducing the predicted X-ray luminosities. In the simulation with mechanical feedback, gas particles are given fixed kick velocities of  $10,000$  km s $^{-1}$ , suggesting that the kinematics of the gas in groups and clusters might also be an important test of models.

The Mg II  $\lambda\lambda 2796,2803$  absorption doublet observed in quasar spectra traces low-ionization gas over a broad range in HI column density ( $10^{16.5} < N_{HI} < 10^{21.5}$  cm $^{-2}$ ). Since the early exploratory work in the late 1980's (Bergeron 1986; Sargent, Steidel & Boksenberg 1988), Mg II has evolved into a useful probe of the gaseous halos around galaxies thanks to very large samples of MgII systems that have been extracted from quasar spectra observed as part of the Sloan Digital Sky Survey (Lundgren et al 2009; Quider et al 2011; Zhu & Ménard 2013; Pérez-Ràfols et al 2015). There have been many studies of the spatial clustering of Mg II systems around massive galaxies observed as part of the Baryon Oscillation Spectroscopic Survey (BOSS; Dawson et al. 2013), which have median stellar masses  $\sim 10^{11.5} M_{\odot}$ . Of particular note is the study of Zhu et al (2014), where the average cool gas surface density profile traced by MgII systems around massive galaxies was measured out to projected radii of 10 Mpc. A change of slope is observed on scales of 1 Mpc, consistent with the expected transition from the regime where the gas is typically within the same dark matter halo as the galaxy, to the regime where the gas is outside the parent halo. Zhu et al introduce a model where the gas distribution is assumed to trace the dark matter distribution exactly, i.e. the gas density profile in a halo of mass  $M$  has the same NFW shape as the dark matter up to a normalization factor  $f_{gas}(M_{halo})$ . This model is shown to provide an adequate fit to the data if the average host halo mass of the galaxies is  $10^{13.5} M_{\odot}$ .

In principle, more stringent constraints on the distribution of gas within dark matter halos can be obtained if the clustering amplitude of MgII systems around galaxies is studied both as a function of projected radius  $R_p$  and as a function of velocity separation  $\Delta V$ . Wild et al (2008) were the first to study both the transverse and the line-of-sight clustering of a large sample of many thousands of CIV and MgII absorption line systems around quasars using data from the SDSS data release 3. These authors found a non-zero correlation between CIV systems and quasars in the redshift interval  $0.4 < z < 2.2$ , extending out to line-of-sight

velocity separations of  $12,000$  km s $^{-1}$ , which could not be explained by assuming that these systems were associated with the foreground galaxy population. They proposed that the high velocity CIV systems instead represented an *out-flowing gas component* that was directly associated with the quasar itself. There was also evidence that high velocity CIV absorbers were more numerous around radio-loud quasars compared to radio-quiet quasars. The sample of MgII absorbers was much smaller than the sample of CIV absorbers, so although there was also a hint of an excess high velocity component of gas traced by MgII, it could not be as accurately quantified.

In this paper, we make use of the galaxy, quasar and quasar absorption line catalogues from the SDSS DR12 (the final data release of the BOSS survey) to compare the line-of-sight clustering of MgII absorbers around massive galaxies, quasars and radio-loud AGN in bins of projected radius from  $R_p = 100$  kpc to  $R_p = 15$  Mpc over the redshift interval 0.4 to 0.75. We interpret our results using full cosmological N-body simulations of dark matter plus gas from the publicly available Illustris simulation (Nelson et al 2015). The N-body+gas simulations incorporate recipes for how AGN heat the gas in and around galaxies. Our paper is structured as follows. In Section 2, we describe the data sets, the construction of our catalogues, and the methodology used for computing the clustering signal. Our empirical results are presented in Section 3 and Section 4 attempts to further interpret these results using simulations.

## 2 SAMPLES AND METHODS

### 2.1 The galaxy sample

The sample of massive galaxies used in this work originates from the twelfth data release (DR12) of the SDSS. Spectra of about 1.5 million galaxies are available from the Baryonic Oscillation Spectroscopic Survey (BOSS; Dawson et al 2013). We select a subsample of galaxies that meet the CMASS target selection criterion, which was designed to select an approximately stellar mass limited sample at  $z > 0.45$ . The sample is defined using the following cuts:

$$17.5 < i < 19.9 \quad d_{\perp} > 0.55 \quad (1)$$

$$i < 19.86 + 1.6(d_{\perp} - 0.8) \quad r - i < 2 \quad i_{fibre} < 21.5 \quad (2)$$

where  $d_{\perp}$  is a ‘rotated’ combination of colours defined as  $d_{\perp} = (r - i) - (g - r)/8$ . This constraint identifies galaxies that lie at high enough redshift so that the 4000 Å break has shifted beyond the observer frame  $r$ -band.  $i_{fibre}$  is the amount of light that enters the fibre. We note that all colour cuts are defined using “model” magnitudes, whereas magnitude limits are given in terms of “cmodel” magnitudes.

We extract a sample of 937,079 galaxies that satisfy the CMASS sample selection cuts and that have redshifts in the range  $0.4 < z < 0.75$  (the lower limit is fixed by the detectability of MgII systems in SDSS quasar spectra and the upper limit by the magnitude limit of the CMASS galaxies (Zhu & Ménard 2013)). In this paper we work with stellar masses and estimates of the 4000 Å break index derived using methods based on principal component analyses (see Chen et al 2012 for more details). These methods are designed to maximize the information content in low  $S/N$

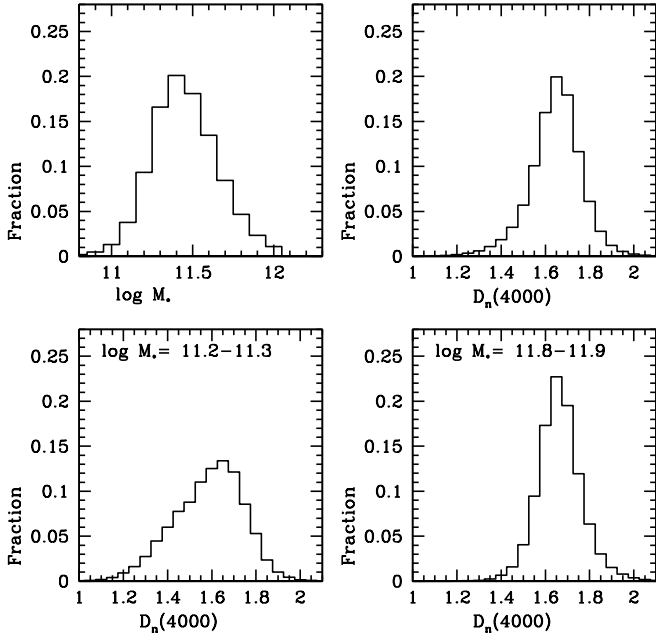


**Figure 1.** *Top left:* Stellar mass distribution of the galaxies in our sample. *Top right:* Estimated 4000 Å break strength distribution of the galaxies. *Bottom panels:* Estimated 4000 Å break strength distributions in two stellar mass ranges.

spectra and they have been shown to reproduce stellar mass estimates based on broad-band photometry and direct measurements of the 4000 Å break in high  $S/N$  spectra of SDSS galaxies at low redshifts. The distribution of stellar masses and 4000 Å break strengths of the galaxies in our sample is shown in the top two panels of Figure 1. The galaxies in our sample lie in the stellar mass range  $10^{11} < M_* < 10^{12} M_\odot$  and the median mass is around  $3 \times 10^{11} M_\odot$ . The distribution of 4000 Å break strengths indicates that the galaxies are predominantly composed of old stars – a single burst of star formation at very high redshift followed by passive evolution yields a 4000 Å break strength of 1.7 at this redshift (assuming solar metallicity), while constant star formation over a Hubble time yields a 4000 Å break strength of 1.4. Significant tails of galaxies with young stars are, however, seen for galaxies with stellar masses closer to  $10^{11} M_\odot$  (lower left panel). As discussed in Chen et al (2012), the fraction of massive galaxies ( $\log M_* > 11.2$ ) with active star formation evolves strongly with redshift, decreasing by a factor of  $\sim 5$  from  $z = 0.6$  to  $z = 0.1$ .

## 2.2 The MgII absorber sample

We begin with a catalogue of 52,243 MgII absorbers extracted from 142,012 quasar spectra from the DR12. Of these, 11035 MgII absorbers have redshifts that overlap the CMASS galaxy sample. The details of the absorption-line detection algorithm are given in Zhu & Menard (2013). The algorithm consists of the following steps:

- (i) continuum estimation using a basis set of eigenspectra
- (ii) filtering out fluctuations on intermediate scales
- (iii) a search using a multi-line model that includes MgII

$\lambda\lambda$  2796, 2803 and 4 strong FeII lines:  $\lambda$  2344,  $\lambda$  2382,  $\lambda$  2586 and  $\lambda$  2600. The inclusion of the Fe II lines eliminates the fraction of false positives by reducing confusion in the case of quasars with multiple absorption-line systems.

(iv) double-Gaussian profile fitting of the MgII  $\lambda\lambda$  2796, 2803 doublet. The dispersions of the two Gaussians are assumed to be identical, but their centers and amplitudes are free parameters in the fitting algorithm. Candidates are rejected if the separation between the Gaussians differs from the fiducial value by more than  $1 \text{ \AA}$

(v) Estimation of the absorber redshift and the rest-frame equivalent widths of the lines.

Zhu & Menard (2013) carry out tests of the completeness of their detection algorithm by adding simulated absorbers drawn from a distribution of rest equivalent widths and doublet ratios. The completeness is higher for stronger absorbers and at redshifts for which the noise level of the flux residuals is lower. Low completeness spikes are found in the region of prominent sky lines and in the wavelength region where data from the red and blue arms of the spectrograph are joined. These completeness estimates are used to correct the observed numbers of absorbers and to derive the differential incidence rate  $dN/dz$  as a function of rest equivalent width. The incidence rate of weaker absorbers with  $0.6 < W_0^{\lambda 2796} < 1.0 \text{ \AA}$  is consistent with constant co-moving density. The incidence of stronger absorbers increases by a factor  $\sim 3$  out to redshifts of 2, before dropping.

## 2.3 Random galaxy catalogues

The goal of the analysis is to quantify the clustering amplitude and spatial extent of the MgII absorbers associated with massive galaxies as a function of projected radius  $R_p$  and velocity separation  $\Delta V$ . In similar fashion to the analysis in Wild et al (2008), we implement a method for computing the excess number of galaxy-absorber pairs relative to an unclustered sample of galaxies.

This is done by computing the number of absorbers expected at random along the actual sightlines used to find the observed pairs. To do this, we create random galaxy samples by randomizing the positions of the galaxies on the sky, but also making sure that the galaxies lie within the boundaries of the CMASS galaxy sample. The redshift of each object is drawn at random from the redshift distribution of the CMASS sample, i.e. the galaxies in the random catalogue and the CMASS sample have exactly the same redshift distributions. This procedure accounts for the evolving number density of MgII absorbers with redshift and the fact that the detection completeness varies as a function of wavelength. The procedure is also straightforward to implement in N-body simulations, as we discuss in Section 4. We have not implemented detailed survey masks, i.e. we have not accounted for the fact that there may be areas within the boundaries of the survey where galaxies are not targeted due to the presence of bright stars, asteroid trails and other imaging imperfections. As we will show, this may introduce a spurious excess clustering signal of  $\sim 10\%$  on the largest scales, but does not affect our primary conclusions.

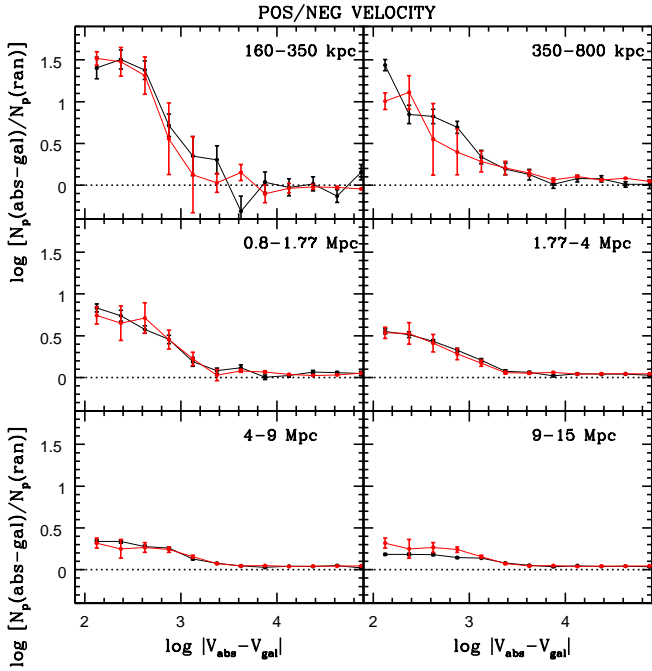


**Figure 2.** The logarithm of the number of galaxy-absorber pairs in the CMASS sample divided by the average number of galaxy-absorber pairs in the random catalogues is plotted as a function of velocity separation. Results are shown in 6 different bins in projected radius  $R_p$ . Results for absorbers with negative velocity separations are plotted in black, and for positive velocity separations in red.

### 3 OBSERVATIONAL RESULTS

We first carry out a check to test the robustness of our procedure for estimating the number of randomly associated absorbers along a given sightline, by plotting the clustering signal separately for absorbers with positive and negative velocity separations with respect to their parent galaxies. Results are shown in Figure 2. We plot the logarithm of the number of galaxy-absorber pairs in the CMASS sample divided by the average number of galaxy-absorber pairs in the random catalogues as a function of velocity separation. Results are shown in 6 different bins in projected radius  $R_p$ , ranging from 160 kpc to 15 Mpc.

As can be seen, a positive clustering signal is detected out to 15 Mpc, and out to velocity separations well beyond  $1000 \text{ km s}^{-1}$ . Error bars have been estimated via bootstrap resampling. We generate 30 different random CMASS catalogues, so the error budget is dominated by the small number of close separation quasar-galaxy pairs in the real CMASS catalogue. We find that the clustering signals in the positive and negative velocity directions are consistent within the errors. This gives us confidence that our procedure for normalizing out the “background” absorbers is giving robust results. There is a small (0.05 dex) residual positive clustering signal at large velocity separations that represents the overall systematic error in the construction of our random catalogues.

We then combine the clustering estimates for positive and negative velocity separations to produce the result shown in Figure 3 (provided in tabular form in Table 1). Ex-

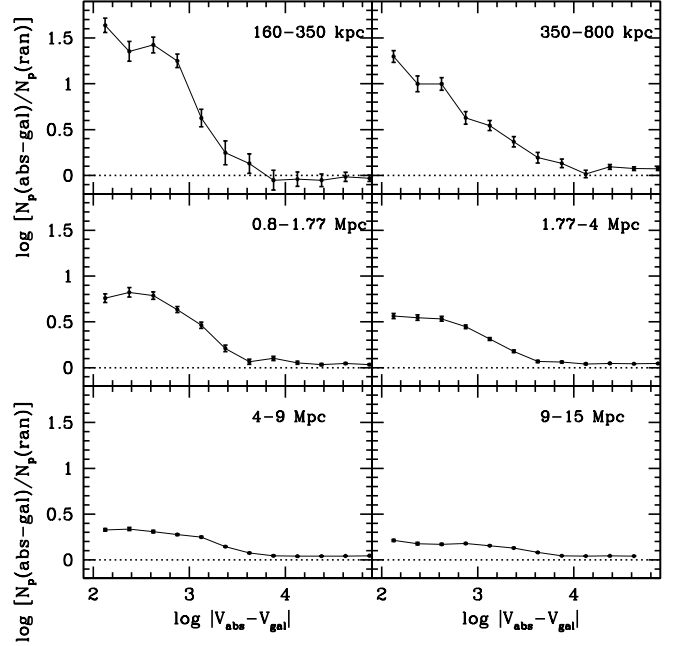


**Figure 3.** The logarithm of the number of galaxy-absorber pairs in the full CMASS sample divided by the average number of galaxy-absorber pairs in the random catalogues is plotted as a function of the absolute value of the velocity separation. Results are shown in 6 different bins in projected radius  $R_p$ .

cess clustering is clearly detected out to velocity separations of  $\sim 10,000 \text{ km s}^{-1}$  in the bins with projected radii less than 800 kpc. At large projected radius, excess absorbers are seen out to velocity separations of  $6000 \text{ km s}^{-1}$ . The clustering amplitude at velocity separations less than  $1000 \text{ km s}^{-1}$  is still nearly a factor of two in excess of the background in the  $R_p = 9 - 15 \text{ Mpc}$  bin.

In Figures 4 and 5, we examine whether the clustering signal shows dependence on galaxy mass or on the age of the stellar population as measured by the  $4000 \text{ \AA}$  break strength. The CMASS sample is divided into two equal high/low mass subsamples at  $\log M_* \sim 11.5$  and into red/blue subsamples at a  $4000 \text{ \AA}$  break strength of 1.7. As can be seen a dependence on galaxy properties is largely absent. MgII absorbers are slightly more numerous around blue galaxies compared to red galaxies in the smallest bin in projected radius (160-350 kpc). Lan, Menard & Zhu (2014) have used photometric catalogues from SDSS and the Galaxy Evolution Explorer (GALEX) satellite to extract a much larger sample of galaxy-absorber close pairs spanning a wide range in galaxy colour. They also find that differences in MgII covering fractions only become significant at small projected radii and most of their analysis is restricted to galaxy-absorber pairs with separations less than 50 kpc. There are only a handful of galaxy-absorber pairs in our sample with such small separations. Note also that the galaxy sample spans a very limited range in stellar mass ( $10^{11} - 10^{12} M_\odot$ ) where the relation between galaxy mass and halo mass is very shallow, so it is perhaps not surprising that there is little dependence of the clustering signal on stellar mass.

Finally, in order to make contact with the analysis of

**Table 1.** The logarithm of the number of galaxy-absorber pairs in the full CMASS sample divided by the average number of galaxy-absorber pairs in 30 random samples is tabulated as a function of velocity separation for the six bins in projected radius in Figure 3

$\log \Delta V$	0.16-0.35 Mpc	0.35-0.8 Mpc	0.8-1.77 Mpc	1.77-4 Mpc	4-9 Mpc	9-15 Mpc
2.125	1.638±0.078	1.299±0.064	0.760±0.047	0.563±0.029	0.328±0.015	0.213±0.011
2.375	1.354±0.108	0.999±0.087	0.821±0.052	0.546±0.030	0.337±0.017	0.177±0.014
2.625	1.424±0.087	0.999±0.069	0.786±0.041	0.533±0.027	0.309±0.015	0.170±0.010
2.875	1.250±0.074	0.628±0.068	0.634±0.033	0.446±0.022	0.276±0.010	0.179±0.008
3.125	0.626±0.096	0.544±0.054	0.464±0.034	0.312±0.016	0.249±0.009	0.155±0.005
3.375	0.247±0.130	0.367±0.056	0.210±0.035	0.178±0.014	0.144±0.006	0.130±0.005
3.625	0.130±0.107	0.193±0.058	0.063±0.028	0.068±0.012	0.076±0.006	0.081±0.003
3.875	-0.053±0.108	0.132±0.046	0.101±0.023	0.060±0.009	0.045±0.004	0.045±0.003
4.125	-0.042±0.077	0.015±0.040	0.053±0.018	0.040±0.007	0.040±0.004	0.042±0.002
4.375	-0.052±0.069	0.092±0.027	0.033±0.013	0.047±0.006	0.041±0.003	0.044±0.002
4.625	-0.016±0.049	0.074±0.021	0.046±0.010	0.042±0.005	0.042±0.002	0.042±0.001
4.875	-0.032±0.035	0.072±0.017	0.034±0.009	0.045±0.003	0.046±0.002	0.042±0.001

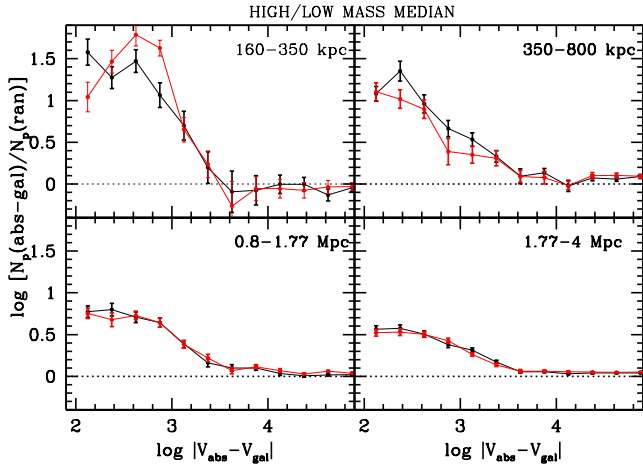


**Figure 4.** The logarithm of the number of galaxy-absorber pairs in the full CMASS sample divided by the average number of galaxy-absorber pairs in the random catalogues is plotted as a function of velocity separation. Results are shown for galaxies with  $\log M_* < 11.5$  in black and for  $\log M_* > 11.5$  in red.

Wild et al (2008), we have carried out similar clustering analysis of MgII absorbers around SDSS quasars. We have also examined clustering of Mg II around galaxies with radio-loud nuclei in the same redshift range ( $0.4 < z < 0.75$ ) as the CMASS sample.<sup>1</sup> To find radio-loud galaxies, we cross-match the CMASS sample with the source catalog from the Faint Images of the Radio Sky at Twenty-Centimeters (FIRST) survey carried out at the VLA (Condon et al. 1998). The SDSS and FIRST positions are required to be within 3 arcseconds of each other. Because radio loud nuclei are known to be biased towards the very most massive galaxies (Best et al 2005), we also extract a ‘control’ sample of galaxies with the same stellar mass distribution that are selected without regard to their radio properties. We note that we do not impose a flux limit on our radio loud galaxy sample as we wish to maximize the number of sources included in the clustering analysis. Inclusion of false detections will act to dilute clustering differences compared

<sup>1</sup> Note that the Wild et al analysis is for radio-loud quasars rather than galaxies

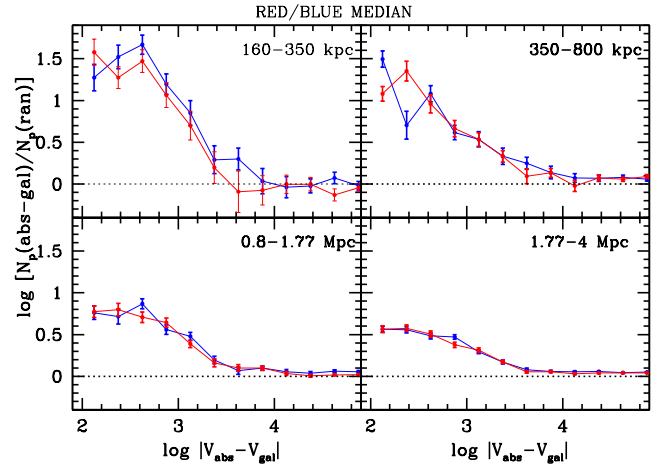


**Figure 5.** The logarithm of the number of galaxy-absorber pairs in the full CMASS sample divided by the average number of galaxy-absorber pairs in the random catalogues is plotted as a function of velocity separation. Results are shown for galaxies with 4000 Å break index strength less than 1.7 in blue and greater than 1.7 in red.

to the control sample. There are 43,812 galaxies in the radio loud galaxy sample. We also select a sample of 18,338 quasars in the same redshift interval from the SDSS DR12 quasar catalogue (Pâris et al. 2016). Because the light from the central nucleus outshines the underlying host galaxy in quasars, we are unable for construct a sample of normal galaxies matched in stellar mass for this sample.

In the left-hand panels in Figure 6, we compare the clustering of MgII absorbers around radio-loud galaxies with the control sample of galaxies matched in stellar mass. As can be seen, the distribution of MgII systems as a function of velocity separation is the same around radio-loud galaxies as it is around normal galaxies. Both samples exhibit clear excess of MgII absorbers out to velocity separations of  $\sim 10,000$  km s<sup>-1</sup>. It is the *amplitude* of the clustering signal of MgII absorbers that is higher around radio-loud galaxies, indicating that there is more cool gas around these systems. In the right hand panel, we compare the clustering of MgII absorbers around radio-loud galaxies and quasars. The results for the quasar sample are quite a lot noisier because of the smaller sample size. We find no clear differences in

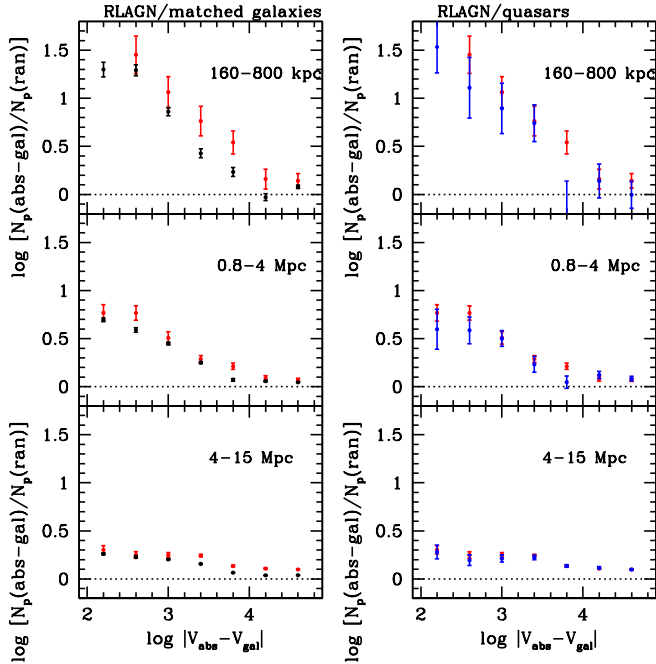


**Figure 6.** *Left panels:* the line-of-sight clustering of MgII absorbers around radio-loud galaxies (red) is compared with the control sample of galaxies matched in stellar mass (black). Results are shown for 3 bins in projected separation. *Right panels:* The clustering of MgII absorbers around radio-loud galaxies (red) and quasars (blue).

the distribution of MgII gas around radio-loud galaxies and quasars.

Our examination of differences in the clustering of MgII systems around galaxies with different 4000 Å break strengths and around quasars and radio-loud galaxies do not support a scenario in which the high velocity gas components are intrinsic to an active galactic nucleus that is instantaneously ejecting gas at very high velocity. If so, one might expect that no high velocity gas components be found around passive galaxies with no AGN. As we will discuss in the next section, our results suggest that the high-velocity MgII absorbers trace gas that has been *pushed out* of galactic halos at some time in the past. This hypothesis is also supported by the fact that the high velocity separation absorbers are not confined to the bins with small projected separation from the parent galaxy, but are seen out to projected radii of tens of Mpc. We come back to this point in the final section.

#### 4 MODELS

In this section, we attempt some simple interpretation of our results with the help of cosmological simulations that also incorporate gas dynamics. A full accounting of observational selection effects is beyond the scope of this paper. To do this, we would need to generate mock quasar absorption line spectra from the simulations and take into account the observed MgII detection thresholds in the data (see Hernquist et al 1996 for discussion of how to generate mock quasar spectra and Ford et al 2016 for discussion of how mock quasar

spectra from simulations can be used in the interpretation of metal absorption line data from the COS-HALOS survey).

The approach we take is similar to that of Zhu et al (2014), except we use simulations rather than analytic models to predict the clustering signal, given a set of possible assumptions for how the MgII gas might trace the underlying large scale structure dominated by cold dark matter. The main advantage of simulations over analytic models is that we can account for large-scale structure present *outside* the virial radius of the dark matter halo. This is necessary in order to address the question of whether high velocity tails of MgII absorbers can be explained in a simple way, or whether we need to invoke models in which AGN feedback significantly alters the structure and kinematics of the gas.

We make use of simulation data released by the Illustris and Millennium cosmological simulation projects. The reader is referred to <http://www.illustris-project.org/> and Nelson et al (2015) for detailed information about the Illustris project and to <http://wwwmpa.mpa-garching.mpg.de/millennium/> and Lemson et al. (2006) for information about the Millennium simulation.

We first show results using dark matter particle and gas data from the Illustris-3 simulation and dark matter subhalo data from the Illustris-1 simulation at an output time that corresponds to the median redshift of the CMASS sample ( $z = 0.55$ , snapshot 101). All the simulations are within a periodic box of length 106.5 Mpc. The dark matter particle mass in the Illustris-3 simulation is  $\sim 4 \times 10^8 M_\odot$ . The average gas cell mass is  $8.1 \times 10^7 M_\odot$ . The Illustris-1 simulation has the same box size, but is run with a dark matter particle mass of  $7.5 \times 10^6 M_\odot$ . The Illustris-3 simulation is used to investigate models where the MgII absorber population is assumed to trace the dark matter or gas distributions. The Illustris-1 simulation is used to investigate models where the MgII absorber population traces dark matter subhalos. The higher resolution is needed so that we can track subhalos down to low masses within groups and clusters. In low resolution simulations, low mass subhalos are tidally disrupted more easily.

We investigate the following simple tracer models and show comparisons with the observational data in Figure 7:

- (i) absorbers trace the dark matter particle distribution (red curves in Figure 7)
- (ii) absorbers trace dark matter subhalos down to some limiting mass (dotted magenta and red curves in Figure 7 show results for limiting masses of  $10^{7.5}$  and  $10^{8.5} M_\odot$ , respectively)
- (iii) absorbers trace the total gas distribution (blue curves in Figure 7)
- (iv) absorbers trace the neutral gas distribution (cyan curves in Figure 7). Neutral gas fractions are read directly from the Illustris simulation.
- (v) absorbers trace gas with  $T < 10^5$  K (green curves in Figure 7), for which the MgII mass fraction is high (see below).

In order to mimic the observational set-up, we select galaxies from the Illustris-1 and Illustris-3 simulations with stellar masses in the range  $10^{11} - 10^{12} M_\odot$ . There are 150 such galaxies in the Illustris-3 simulation and 369 in Illustris-1. The larger number of massive galaxies in Illustris-1 is the

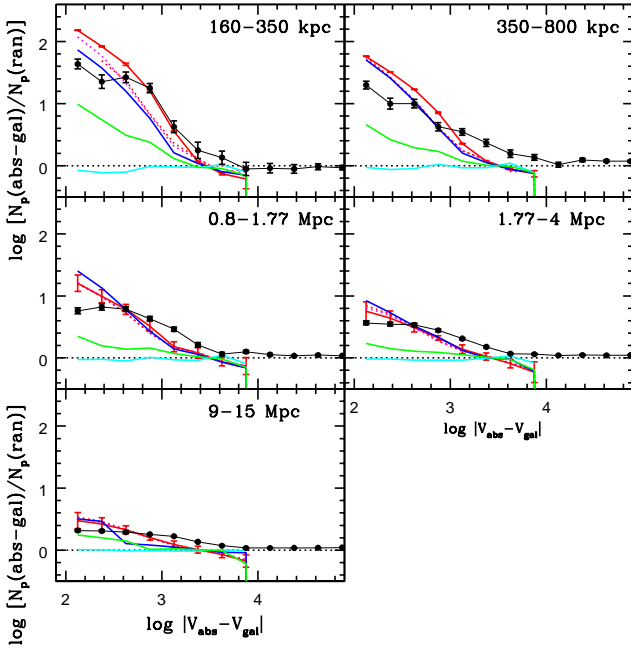


**Figure 7.** Line-of-sight clustering predictions for different tracer models are compared to the observational data. Please see the text for details of the different models. Black curves show the same data as in Figure 3. Solid red curves are for a model where the absorbers trace the dark matter particle distribution. Dotted red and magenta curves are models where the absorbers trace the dark matter subhalo population. Cyan curves are for a model where the absorbers trace the neutral gas component. Green curves are for a model where the absorbers trace gas with temperature  $T < 10^5$  K.

result of enhanced cooling of gas in high density regions that are more highly resolved. As discussed in Vogelsberger et al (2014), there is an excess of massive galaxies compared to observations in Illustris-1 of about a factor of two at stellar masses of  $\sim 10^{11.5} M_{\odot}$ .

Results for all the Illustris tracer models are shown in Figure 7. The models where absorbers trace the dark matter, the dark matter subhalo population or the total gas distribution all lie above the observations at small velocity separations ( $\Delta V < 500$  km/s), and then fall below the data at  $\Delta V > 1000$  km/s. The model where absorbers trace the neutral gas distribution shows no enhancement of neutral gas around massive galaxies compared to random sightlines. This is because the galaxies in our sample typically reside in dark matter halos of masses  $\sim 10^{13} M_{\odot}$  or greater, where most of the gas in the halo has been shock-heated to high enough temperatures to ionize almost all the hydrogen. In addition, “radio-mode” AGN feedback following Sijacki et al (2007) where bubbles of hot gas with radius 50 kpc, total energy  $10^{50}$  erg are placed within the halo, also acts to stop gas from cooling in halos of this mass.

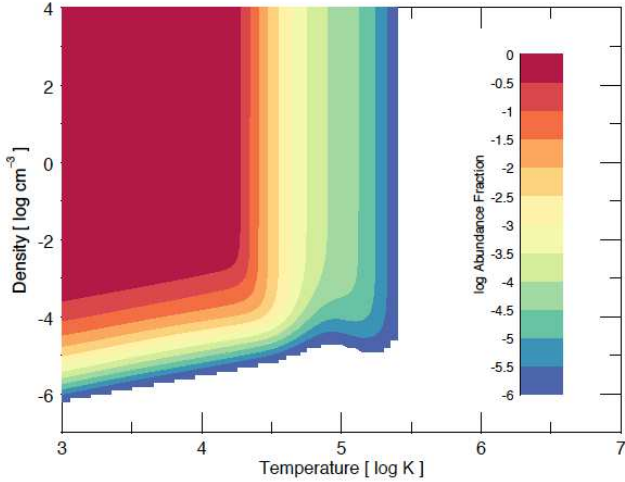
The tracer model that comes closest to mimicking how MgII absorbers might be distributed in the Illustris simulation is the model where absorbers trace gas with  $T < 10^5$  K. This is illustrated in Figure 8, which shows, as a function of density and temperature, where the dominant fractions of Magnesium are in the form of Mg II. To compute these ionic

abundances we use CLOUDY (v13.03, Ferland et al. 2013) including both collisional and photo-ionization in the presence of a UV background (Ferland 2009). We follow Bird et al. (2015) and use CLOUDY in single-zone mode, accounting for a frequency dependent shielding from the background radiation field at high densities, using the fitting function of Rahmati et al. (2013). Under these assumptions MgII is found predominantly in gas with densities above  $10^{-4} \text{ cm}^{-3}$  and temperatures below  $10^5$  K. The MgII fractions are also roughly constant in this regime. As can be seen from Figure 7 (green curves in the plot), in this model, MgII absorbers are significantly more clustered around massive galaxies than in random sightlines, but the amplitude is lower than in the observations. In addition, there is no tail to large velocity separations as in the data.

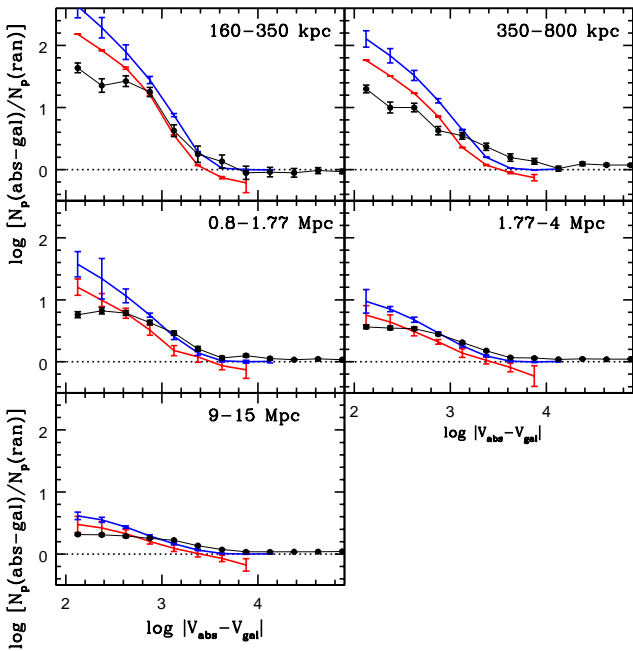
In order to evaluate the clustering out to velocity separations of 10,000 km/s in the Illustris simulation, we have replicated the simulation box periodically in the x,y and z directions. We caution that missing large scale power will result in an under-prediction of the clustering amplitude at large velocity separations comparable to the box size. In addition, the integral constraint on the correlation function also implies that clustering at large velocity separations will be under-estimated. In order to investigate this, we compare results for the Illustris tracer model (i) with results obtained for the Millennium simulation, which has a box size  $500h^{-1}$  Mpc, i.e. 6.7 times larger than the Illustris box. Once again, we select galaxies with stellar masses in the range  $10^{11} - 10^{12} M_{\odot}$  from the  $z = 0.5$  snapshot to represent the galaxy population. We note that unlike Illustris, the parameters of the galaxy formation models in the Millennium simulations are tuned to provide an accurate fit to the galaxy luminosity function. In particular, the volume density of massive galaxies predicted by the Millennium simulation is in much better agreement with observational constraints than in Illustris (Croton et al 2006).

Figure 9 shows that clustering amplitude predicted by the Millennium dark matter model is significantly higher than that predicted by Illustris. As we have discussed, the Illustris simulation overproduces massive galaxies and they thus will trace dark matter halos with lower masses, leading to a lower clustering amplitude prediction. The Millennium dark matter model also converges cleanly to zero overdensity at large velocity separations, indicating that box size is now sufficiently large. The model provides a better match to the clustering amplitude at large  $\Delta V$  in the bins with large projected radius. We see that there is still a significant tail of high velocity MgII absorbers in the 350-800 kpc bin. The interpretation of the size of the excess is compromised by the fact that the Millennium model overshoots the clustering amplitude at small  $\Delta V$  by such a large factor.

In summary, none of the models explored in this section provide an adequate fit to the observational data. Models in which the MgII absorbers trace the dark matter are too highly clustered at small velocity separations. This is in agreement with the conclusions of Wild et al (2008). There appears to be a significant high velocity tail of absorbers that is especially apparent at projected radii between 300 -800 kpc, which cannot be reproduced by any of the models explored in this paper. It will be interesting to see whether the large  $\Delta V$  problem will be resolved in models with black hole driven thermal and kinetic feed-



**Figure 8.** The fraction of Magnesium in the form of Mg II as a function of density and temperature as predicted by CLOUDY in single-zone mode, including both collisional and photo-ionization in the presence of a UV background (see text).



**Figure 9.** Line-of-sight clustering predictions for the dark matter tracer model in the Illustris simulation (red) is compared to that for the Millennium simulation (blue). The observational data are shown as black points.

back (e.g. Weinberger et al 2016). It also remains to be seen whether the MgII absorber population predicted by applying CLOUDY photo-ionization models to simulations that better resolve the small scale structure of the gas, can provide a better fit at small  $\Delta V$ .

## 5 DISCUSSION

In section 4, we showed that none of our tracer models were able to account for the clustering signal at large velocity separations from the parent galaxy. In section 3, we proposed that the large  $\Delta V$  absorber population was unlikely to be associated with outflowing material from an active galactic nucleus, because it is detected out to large (at least 1 Mpc) projected radius  $R_p$ . We note that Wild et al. (2008) and all other previous work on associated absorbers only investigated line-of-sight clustering of CIV and MgII absorbers to the host QSO, and only probed the high velocity gas in front of the QSO. Wild et al. additionally measured the transverse clustering of the absorbers around the QSOs, but did not investigate the velocity distribution of this gas.

It is also interesting to investigate how far out in projected radius we are able to detect a clustering signal. In Figure 10, we show the number of absorber-CMASS galaxy pairs divided by the number of absorber-random galaxy pairs is plotted in 3 bins of projected radius: 4-9 Mpc, 9-20 Mpc, and 20-45 Mpc. Results are shown for 4 different bins in stellar mass  $M_*$ . Note that the y-axis in this plot is in linear rather than logarithmic units, in order to see the extent of the low amplitude clustering signal more clearly. A significant excess of MgII absorbers is detected out to velocities well beyond 3000 km/s even in the 9-20 Mpc bin. The excess clustering has largely disappeared at all velocity separations in the 20-45 Mpc bin.

One possible interpretation of our results is that the MgII absorbers with large  $\Delta V$  trace gas that has been pushed out of dark matter halos. A series of papers (Kauffmann et al 2013; Kauffmann 2015) have investigated an interesting large-scale clustering phenomenon that we now propose may be closely related. In brief, it has been found that the correlation between the colours and specific star formation rates of neighbouring galaxies first noticed by Weinmann et al (2006) and dubbed “galactic conformity”, extends far beyond the scale of the virial radii of their dark matter halos. In particular, Kauffmann (2015) showed that low mass galaxies with low specific star formation rates are surrounded by neighbouring galaxies with lower than average specific star formation rates out to projected radii of  $\sim 20$  Mpc, which is very similar to the scales over which we find the excess MgII absorber population. The interstellar medium of low mass galaxies travelling through large-scale reservoir of gas with temperatures of  $10^5 - 10^6$  K may be stripped by ram-pressure forces, leading to a shut-down in star formation that is correlated over scales of many Mpc, as seen in the data.

Kauffmann (2015) also find a significant excess of very high mass ( $\log M_* > 11.3$ ) galaxies around low  $SFR/M_*$  central galaxies and an even larger excess of high mass galaxies hosting radio-loud AGN around these systems. This again suggests a link between the large-scale MgII absorber excess and the galactic conformity phenomenon. As shown in Figure 6, the number of MgII systems around radio-loud AGN is significantly higher than in control samples of the same stellar mass, which probably implies that the total gas density is higher in the vicinity of radio-loud AGN and that ram-pressure stripping effects on low mass galaxies will be more pronounced.

The final question we address is what physical process is

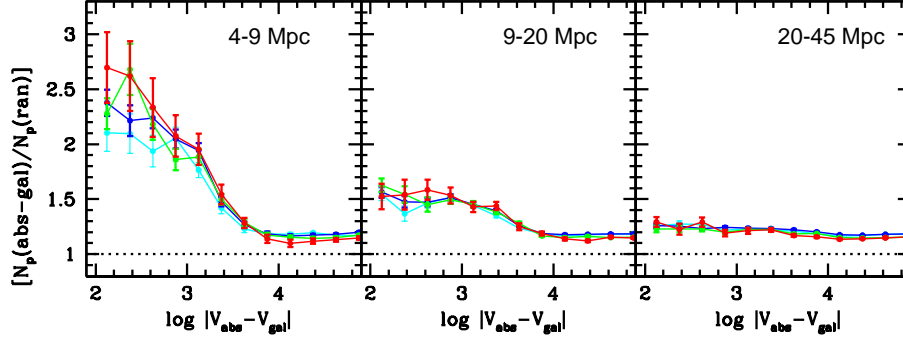


**Figure 10.** The number of galaxy-absorber pairs divided by the average number of galaxy-absorber pairs in the random catalogues is plotted as a function of velocity separation. Results are shown in 3 different bins in projected radius  $R_p$  from 4 to 45 Mpc. Different colour curves show results for different stellar mass intervals:  $10^{11} - 10^{11.2} M_{\odot}$  (cyan),  $10^{11.2} - 10^{11.4} M_{\odot}$  (blue),  $10^{11.4} - 10^{11.6} M_{\odot}$  (green),  $10^{11.6} - 10^{11.8} M_{\odot}$  (red).

responsible for pushing gas out of galactic halos. We do not find any correlation between the presence of a population of large velocity separation absorbers and a radio-loud active galactic nucleus. This does not rule out the possibility that excess gas on large scales may have been pushed out of the halo by *multiple episodes* of AGN feedback over timescales of many Gyr. Tremonti et al (2007) obtained spectra of 14 massive galaxies with  $M_* \sim 10^{11} M_{\odot}$  and redshifts similar to the CMASS galaxies in our sample. In 10/14 cases, the MgII  $\lambda 2796, 2803$  absorption lines were blue-shifted by 500-2000 km/s with respect to the stars. Chen et al (2013) have carried out an analysis of the star formation histories of CMASS galaxies and find that the spectra of galaxies with ongoing star formation are best fit by models that include recent bursts. This motivates us to search for a sub-population of MgII systems at small impact parameters that have been ejected more recently.

Two properties of the MgII absorber systems are available from the catalogue of Zhu & Ménard (2013): the absorption line equivalent width and the doublet ratio  $W_0^{2796}/W_0^{2803}$ . We extract all MgII absorbers within a projected radius of 500 kpc from a CMASS galaxy, and we plot the doublet ratio and the equivalent width of the  $\lambda 2796$  MgII line as a function of velocity separation in the left-hand panels of Figure 10. In the right-hand panels, we plot doublet ratio and equivalent width as a function of  $R_p$  for all absorbers within  $\Delta V < 10,000$  km/s. The red error bars indicate the running median of the distribution, while the green error bars indicate the upper 75th percentile. There is no trend in either equivalent width or doublet ratio as a function of  $R_p$  for the population of absorbers as a whole. We note, however, that we cannot extend our analysis to  $R_p$  smaller than 100 kpc, because of poor sample statistics. The top left panel of Figure 11 provides an interesting hint that the population of high velocity MgII absorbers located at small impact parameters may be systematically different from the absorbers associated within the galaxy’s halo. There is a decrease in doublet ratio as a function of  $\Delta V$  from  $\Delta V = 50$  km/s out to  $\Delta V = 700$  km/s, followed by a flat relation out to very large velocity separations. Note that

$\Delta V = 700$  km/s corresponds reasonably well to the boundary expected for gas clouds that are in virial equilibrium within dark matter halos in the mass range  $10^{13} - 10^{14} M_{\odot}$ . The  $W_0^{2796}/W_0^{2803}$  ratio is expected to be bounded between 2 (the optically thin regime) and 1 (saturated). If the low  $\Delta V$  MgII absorbers correspond to gas clouds that are in virial equilibrium within the inner regions of the halo, they may be more optically thin because ram-pressure and tidal forces, as well as collisional heating processes, have acted to reduce their column densities.

In future work, we plan to analyze MgII  $\lambda 2796, 2803$  absorption in the actual spectra of CMASS galaxies and see whether we can find more robust evidence for outflowing systems. The number of MgII systems observed at small impact parameters is extremely limited in this analysis because both the quasar and the CMASS galaxy samples have low densities on the sky. In future, it will be valuable to increase the coverage in the vicinity of high mass galaxies by targeting background quasars down to fainter limits. Spectroscopic surveys of galaxies in the same redshift range to fainter limiting magnitudes would allow us to study the kinematics of the gaseous halos of galaxies spanning a wide range in stellar mass. Higher resolution, higher signal-to-noise spectra would be valuable in order to understand the physical conditions in the gas traced by the MgII systems in more detail. Finally, more detailed modelling of the MgII absorber population is clearly needed to understand the implications of the observational results in greater depth.

## ACKNOWLEDGMENTS

We thank Simon White and Philipp Busch for helpful input to the analysis.

## REFERENCES

- Anderson M. E., Gaspari M., White S. D. M., Wang W., Dai X., 2015, MNRAS, 449, 3806  
 Bergeron J., 1986, A&A, 155, L8

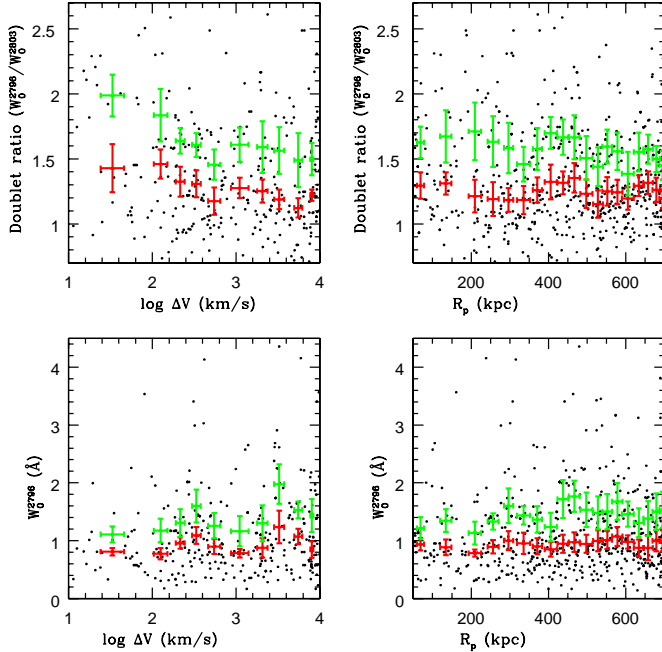


**Figure 11.** *Left panels:* The doublet ratio  $W_0^{2796}/W_0^{2803}$  and the equivalent width  $W_0^{2796}$  is plotted as a function of velocity separation for absorbers with  $R_p < 500$  kpc. Red points with error bars show estimates of the running median. Green points with error bars show the upper 75th percentile points. Error bars have been computed using a standard bootstrap resampling method. *Right panels:* The same two quantities are plotted as a function of projected radius  $R_p$  for absorbers with  $\Delta V < 10,000$  km s $^{-1}$ .

Bird S., Haehnelt M., Neelam M., Genel S., Vogelsberger M., Hernquist L., 2015, MNRAS, 447, 1834  
 Best P. N., Kauffmann G., Heckman T. M., Brinchmann J., Charlot S., Ivezić Ž., White S. D. M., 2005, MNRAS, 362, 25  
 Chen Y.-M., et al., 2012, MNRAS, 421, 314  
 Chen Y.-M., et al., 2013, MNRAS, 429, 2643  
 Choi E., Naab T., Ostriker J. P., Johansson P. H., Moster B. P., 2014, MNRAS, 442, 440  
 Choi E., Ostriker J. P., Naab T., Oser L., Moster B. P., 2015, MNRAS, 449, 4105  
 Condon J. J., Cotton W. D., Greisen E. W., Yin Q. F., Perley R. A., Taylor G. B., Broderick J. J., 1998, AJ, 115, 1693  
 Crenshaw D. M., Kraemer S. B., George I. M., 2003, ARA&A, 41, 117  
 Croton D. J., et al., 2006, MNRAS, 365, 11  
 Dawson K. S., et al., 2013, AJ, 145, 10  
 Ferland G. J., 2009, A&A, 500, 299  
 Ferland G. J., et al., 2013, RMxAA, 49, 137  
 Ford A. B., Oppenheimer B. D., Davé R., Katz N., Kollmeier J. A., Weinberg D. H., 2013, MNRAS, 432, 89  
 Ford A. B., et al., 2016, MNRAS, 459, 1745  
 Hernquist L., Katz N., Weinberg D. H., Miralda-Escudé J., 1996, ApJ, 457, L51  
 Kauffmann G., White S. D. M., Guiderdoni B., 1993, MNRAS, 264, 201  
 Kauffmann G., Li C., Zhang W., Weinmann S., 2013, MN-

RAS, 430, 1447  
 Kauffmann G., 2015, MNRAS, 454, 1840  
 Lan T.-W., Ménard B., Zhu G., 2015, MNRAS, 452, 3629  
 Lemson G., Virgo Consortium t., 2006, astro, arXiv:astro-ph/0608019  
 Lundgren B. F., et al., 2009, ApJ, 698, 819  
 McCarthy I. G., et al., 2010, MNRAS, 406, 822  
 Nelson D., Genel S., Vogelsberger M., Springel V., Sijacki D., Torrey P., Hernquist L., 2015, MNRAS, 448, 59  
 Pâris I., et al., 2016, arXiv, arXiv:1608.06483  
 Pérez-Ràfols I., Miralda-Escudé J., Lundgren B., Ge J., Petitjean P., Schneider D. P., York D. G., Weaver B. A., 2015, MNRAS, 447, 2784  
 Quider A. M., Nestor D. B., Turnshek D. A., Rao S. M., Monier E. M., Weyant A. N., Busche J. R., 2011, AJ, 141, 137  
 Rahmati A., Schaye J., Pawlik A. H., Raičević M., 2013, MNRAS, 431, 2261  
 Sargent W. L. W., Steidel C. C., Boksenberg A., 1988, ApJ, 334, 22  
 Sun M., Voit G. M., Donahue M., Jones C., Forman W., Vikhlinin A., 2009, ApJ, 693, 1142  
 Tremonti C. A., Moustakas J., Diamond-Stanic A. M., 2007, ApJ, 663, L77  
 Vogelsberger M., et al., 2014, MNRAS, 444, 1518  
 Wang W., White S. D. M., Mandelbaum R., Henriques B., Anderson M. E., Han J., 2016, MNRAS, 456, 2301  
 Weinberger R., et al., 2016, arXiv, arXiv:1607.03486  
 Weinmann S. M., van den Bosch F. C., Yang X., Mo H. J., 2006, MNRAS, 366, 2  
 White S. D. M., Frenk C. S., 1991, ApJ, 379, 52  
 Wild V., et al., 2008, MNRAS, 388, 227  
 Zhu G., Ménard B., 2013, ApJ, 770, 130  
 Zhu G., et al., 2014, MNRAS, 439, 3139